Appl. Phys. B 90, 455–460 (2008)
DOI: 10.1007/s00340-007-2854-9

Applied Physics B
Lasers and Optics

A.V. AZAROV
P.J.M. PETERS✉
K.-J. BOLLER

Laser gain measurements at 193 nm in a small discharge cell containing ArF excimer laser gas mixtures

Laser Physics and Nonlinear Optics Group, MESA+ Research Institute, Faculty of Science and Technology, University of Twente, P.O. Box 217, 7500 AE Enschede, The Netherlands

Received: 14 August 2007/Revised version: 23 October 2007
Published online: 18 January 2008 • © The Author(s) 2008

ABSTRACT Spatial and temporal gain profiles as well as the peak net gain at 193 nm have been measured in X-ray preionized discharges excited by a single pulse electrical system working in the charge transfer mode. Ar- and F_2-containing laser gas mixtures with He or Ne as a buffer gas have been used. With a pumping pulse duration of ~ 100 ns (FWHM) and a specific peak power deposition of $\sim 1\,\mathrm{MW\,cm^{-3}\,bar^{-1}}$ in a gas mixture containing $F_2 : Ar : He$ (0.1% : 5% : 94.9%), at 2 bar total pressure, a very high peak net gain coefficient of $\sim 30\%\,\mathrm{cm^{-1}}$ was measured in the gas discharge. The FWHM of the gain waveform was ~ 60 ns.

PACS 42.55.Lt; 42.60.Lh; 52.80.-s

1 Introduction

Excimer lasers are powerful sources of coherent ultraviolet (UV) and vacuum ultraviolet (VUV) radiation. They are used extensively in industry and for scientific research. Industrial applications are found in nano-lithography and material processing such as fast cutting of different materials and drilling of large numbers of small holes in metals and composites, e.g., for use in jet engines turbine blades and aircraft wings. Currently KrF* (248 nm) and ArF* (193 nm) excimer lasers are the most common light sources used in the mass production of integrated circuits in the semi-conductor industry. With the help of a special technique called immersion lithography, sizes of approximately 45 nm and above [1] are obtained using ArF* excimer lasers. Scientific applications include surface-ablation studies and X-ray plasma generation.

Commercially available ArF* lasers usually deliver laser pulses with a typical duration of a few tens of ns. This short optical pulse duration is a drawback found in all existing excimer lasers. Due to such a short pulse duration only a few round-trips inside the laser resonator are possible, resulting in poor optical beam quality. With a longer optical pulse duration, a higher beam quality and therefore greater focusability of the laser beam is obtained. On the other hand, enhancing the optical gain in excimer laser gas mixtures may lead to shorter laser devices. This will allow more roundtrips in the laser resonator and consequently a higher beam quality.

In this paper we present the results of our gain measurements in a small-volume ($\sim 1\,\mathrm{cm^3}$) X-ray preionized gas discharge system that is able to produce long optical pulses (~ 100 ns). In this discharge system a specific power deposition of $\sim 1\,\mathrm{MW\,cm^{-3}\,bar^{-1}}$ and a pumping pulse duration of ~ 100 ns (FWHM) are easily achievable in different excimer gas mixtures, including F_2- containing mixtures. The electrical properties of the gas discharge system in such mixtures were investigated for a wide range of different gas mixtures. In Ar- and F_2-containing mixtures the total optical output and signal amplification at a wavelength of 193 nm (ArF* excimer) were measured.

The highest measured specific peak net gain at 193 nm was found to be $\sim 30\%\,\mathrm{cm^{-1}}$ in mixtures of Ar and F_2 diluted with either in He or Ne. This value is much higher than reported in the literature, where for discharge pumped systems the gain varied from $\sim 3\%$–$10\%\,\mathrm{cm^{-1}}$ [2, 3] to $\sim 17\%\,\mathrm{cm^{-1}}$ [4].

2 Experimental setup and method

The experimental setup is shown in Fig. 1. The discharge chamber consists of a cylindrical quartz tube with inner diameter of 74 mm, two Al flanges and two Al electrodes attached to the flanges. The upper electrode is 50 mm in diameter and serves as an anode. The lower electrode is 60 mm in diameter and serves as a cathode. Both electrodes have rounded edges to prevent enhancement of the electric field and are covered with a thin layer of Ni ($\sim 30\,\mu$m). The lower flange and electrode has a cavity 1 cm in diameter, which forms the input window for the X-ray preionization pulse. The discharge gap between the electrodes is 1 cm.

The X-ray preionization pulse is produced by a homemade vacuum X-ray source. A vacuum corona-plasma cathode similar to the devices described in [5, 6] is used to create an electron beam that converts its energy into X-ray radiation when the e-beam is stopped by a thin Ta foil ($\sim 100\,\mu$m). The output window of the source is shielded by Pb plates to form a collimated X-ray beam 1 cm in diameter. The X-ray source is powered by a homemade 6-stage mini-Marx generator which is charged by an HV dc power supply (Hipotronics R 60A) and triggered by a homemade triggering unit. The typical dose produced inside the gas discharge chamber by

✉ Fax: +31-53-489-1102, E-mail: p.j.m.peters@tnw.utwente.nl

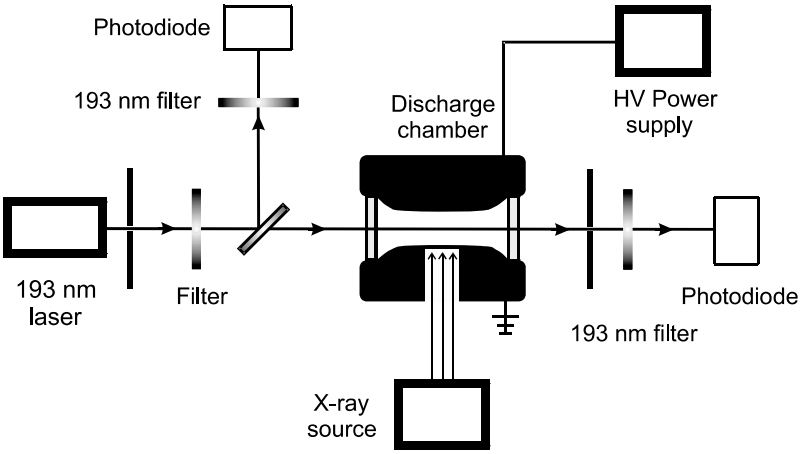

FIGURE 1 Experimental setup

this X-ray source and measured by means of a conventional pen-dosimeter SEQ6 (0.1 rad) is ~ 1 mrad/shot. The specific preionization electron density produced by this X-ray pulse in the discharge chamber was measured previously and was found to be $\sim 10^7$ cm^{-3} bar^{-1} in He.

The HV Power supply contains a high voltage pulse-forming unit including a 1 MΩ load resistance, a 3 nF storage capacitor and A TGI1-1000/25 thyratron as a switch. A 47 kΩ resistance is connected parallel to the discharge chamber and allows charging of the storage capacitor. The pulse forming unit is charged by an HV dc power supply (Hipotronics 8100-10) and the thyratron is triggered by a home-made triggering unit. A fast (> 100 MHz) current transformer and a fast high voltage probe (> 100 MHz) are used to measure the discharge current and voltage waveform.

An ExciStar XS-200 ArF excimer laser made by TuiLaser (Germany) with a 3×6 mm^2 beam cross-section was used as the probe laser for the gain measurements. Two pulse generators (Hewlett-Packard 8003A and Farnell PG102) are coupled and are used as the primary generator to trigger the mini-Marx generator, the discharge and the probe laser, with the appropriate time delays to provide a homogeneous discharge initiation and the temporal scanning of the discharge by the probe laser. The probe laser pulse passes through an aperture which limits the vertical dimension of the laser beam to 5 mm. A neutral density filter attenuates the laser pulse energy approximately 500 times. A semi-transparent mirror splits the laser beam. One part passes through a 193 nm filter LC-193 BP 20 to a control photo-diode FND 100Q. The other part passes through the middle of the discharge chamber, then through an aperture with a variable diameter and via another 193 nm filter LC-193 BP 20 to the signal photodiode UV 444BQ. The second aperture allows control of the amount of the gathered spontaneous emission due to a change of the solid angle.

The signals from both photo-diodes as well as the current and voltage waveforms are captured by a digital oscilloscope Tektronix TDS 640A and processed by a PC. The spontaneous emission waveforms at 193 nm were measured either together with the probe laser signal or alone with the probe laser switched off.

For the measurements of the spatial profile of the laser signal gain, the experimental setup was changed in such a way that the probing laser beam kept the same direction but shifted horizontally through the gain medium. The two diaphragms, the 193 nm filter and the signal detector are moved in the same way as the probe beam. The experimental configuration is shown in Fig. 2. The diameter of the aperture before the discharge chamber determines the spatial resolution and in our experiments it was 0.8 mm. The diameter of the aperture behind the discharge chamber was set in every experiment to provide comparable amplitudes of the spontaneous emission and the probe laser signals measured by the signal photodiode. The diameter of the aperture before the control photodiode was chosen in such a way that the amplitudes of the probe laser signal is comparable on both photodiodes. The photodiodes were calibrated and checked for linearity by means of the probe laser and a Molectron EnergyMax 500 energy meter prior to the experiments. The transmittances of the neutral density filter, both 193 nm filters, the quartz chamber wall and all mirrors used, as well as their reflectances, were measured by means of the probe laser and the same energy meter. We recorded all measurements at a Tektronix TDS 640A oscilloscope with a bandwidth of 100 MHz. The home-made voltage

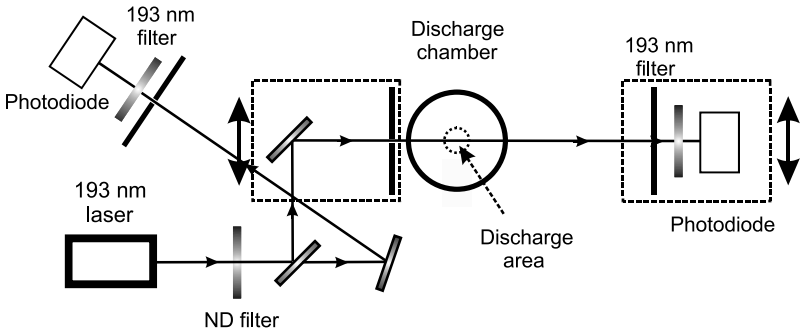

FIGURE 2 Layout of the optical part of the experimental setup for measuring the spatial gain distribution (top view)

probe and current transformer are experimentally proven to have a wider bandwidth (~ 250 MHz).

Prior to the experiments the discharge chamber was evacuated and then filled with a 5% F_2 : He gas mixture at a total pressure of 2 bar and left overnight to passivate the chamber. For the experiments the chamber was evacuated again and filled with the a F_2 : Ar : He or F_2 : He : Ar : Ne gas mixture at the required gas pressure. The charging voltage of the discharge pulse forming unit is adjustable and is usually varied from 8 to 20 kV in order to provide different input energies of the discharge pumping pulse.

In the gain measurements we intentionally observe the probe laser signal on a background of the spontaneous emission of the discharge for two reasons. First, the spontaneous emission signal amplitude is a good indicator of the homogeneity of the gas discharge. If an instability occurs in the discharge, it leads to an instant termination of the spontaneous emission signal. Second, the measured FWHM is ~ 60 ns while the probe laser provides a ~ 10 ns long pulse. Therefore these two signals are easily separable and it is very easy to determine the temporal position of the probe laser pulse from the spontaneous emission waveform.

Each gain measurement consisted of four steps. The first step was to measure the amplitudes of the signals (averaged over ~ 10 shots) from the control (S_c) and signal (S_s) photodiodes with the discharge chamber filled with the working gas mixture but without discharge. This averaged ratio $\langle S_c/S_s\rangle$ refers to the splitting ratio of the beam, the difference in absorption of two beams along their paths and the different sensitivities of the photodiodes. In the second step the probe laser was switched off but the gas discharge was ignited. The signal photodiode measured the spontaneous emission signal ~ 10 times. In this way the averaged spontaneous emission waveform $\langle S_{sp}\rangle$ was determined. In the third step, the signals from the signal and control photodiodes were measured with the probe laser turned on and the discharge ignited. This measured signal by the signal photodiode S_s^+ was then corrected for the average spontaneous emission signal to determine the amplified signal S_s^*:

$$S_s^* = S_s^+ - k\langle S_{sp}\rangle\,. \tag{1}$$

The coefficient k (~ 1) was determined experimentally as the best fit of the spontaneous emission part of the signal S_s^+ by the averaged spontaneous emission waveform multiplied by k before and after the probe laser signal. The control signal S_c^* was measured directly. The ratio S_c^*/S_s^* shows how the previously measured average ratio $\langle S_c/S_s\rangle$ changes due to amplification of the laser pulse or its absorption in the chamber during a discharge.

The spatially averaged net gain along the path L is determined as follows:

$$(g-\alpha)L = -100\%\ln\left(\frac{S_c^*/S_s^*}{\langle S_c/S_s\rangle}\right)\,. \tag{2}$$

In the last step the net gain is calculated from several averaged shots.

By this procedure the spatially averaged net gain along the path of the probe beam was determined. To find the specific net gain in terms of $\%\,\mathrm{cm}^{-1}$ we sent the probe beam through the center of the discharge. The path length L was determined either from the visible width of the discharge or from the width of the spatial gain distribution.

3 Experimental results and discussion

The discharge appears in the middle of the preionized area. At low charging voltages it occupies only the small central part several millimeters in diameter. As the charging voltage increases, the current rises almost linearly, and so does the visible diameter of the discharge. In this region the quasi-steady-state voltage is constant, so the total power deposition also rises linearly. This behavior resembles the well-know normal current density effect for dc discharges. At higher charging voltages the discharge occupies the entire preionized volume, and the diameter of the discharge is then approximately 1 cm, yielding a discharge volume of $0.8\,\mathrm{cm}^3$.

In Fig. 3 typical measured discharge voltage (a) and current (b) waveforms are shown, as well as the calculated power deposition (c) and the spontaneous emission (d) measured by the signal photodiode. A gas mixture containing F_2 : Ar : He (0.1% : 5% : 94.9%) at a total pressure of 2 bar and charging voltage 14 kV was used. The voltage increases until breakdown of the gap, then the voltage almost instantaneously collapses to approximately 4 kV as the discharge is complete (steady state voltage) and then slowly decreases further over time. The current is sinusoidal in shape (in Fig. 3b only a part of the current waveform is shown). In this particular case the current reaches its maximum value at about 100 ns after the initiation of the discharge. In Fig. 3c the power deposition into the discharge is shown. The maximum value is ~ 700 kW and the half-width of the pulse is on the order of 100 ns. The half-width of the spontaneous emission signal is approximately 60 ns and is clearly shorter than the duration of the excitation pulse. The maximum of the spontaneous emission appears approximately at the same time as the maximum of the power deposition. Since we have calibrated the photodiodes by means of the probe laser and have measured the solid angle from which the spontaneous emission is gathered, it is possible to calculate the light intensity in terms of power emitted per unit solid angle. In this case the peak value of the spontaneous emission is approximately $4.5\,\mathrm{kW\,srad}^{-1}$.

The peak power deposition depends on the charging voltage almost linearly, as long as the steady state voltage is constant and the peak current increases linearly with the charging voltage. In Ne-based mixtures the steady state voltage is ~ 2 times lower than in He-based mixtures, as is the peak power deposition because the peak current is almost equal in these two different gas mixtures at the same charging voltage. The peak spontaneous emission signal amplitude for a given gas mixture increases nearly linearly with the peak power deposition until a saturation is reached. The spontaneous emission signal stays constant with a further increase of the power deposition. The saturated emission signal amplitude and the saturation power deposition depend on the gas mixture composition and the total gas pressure.

It is noteworthy that at low power deposition (< 200 kW) the FWHM of the pumping pulse is slightly longer – approximately 140–160 ns. With an increase of the charging voltage the FWHM decreases and at a pumping power deposition

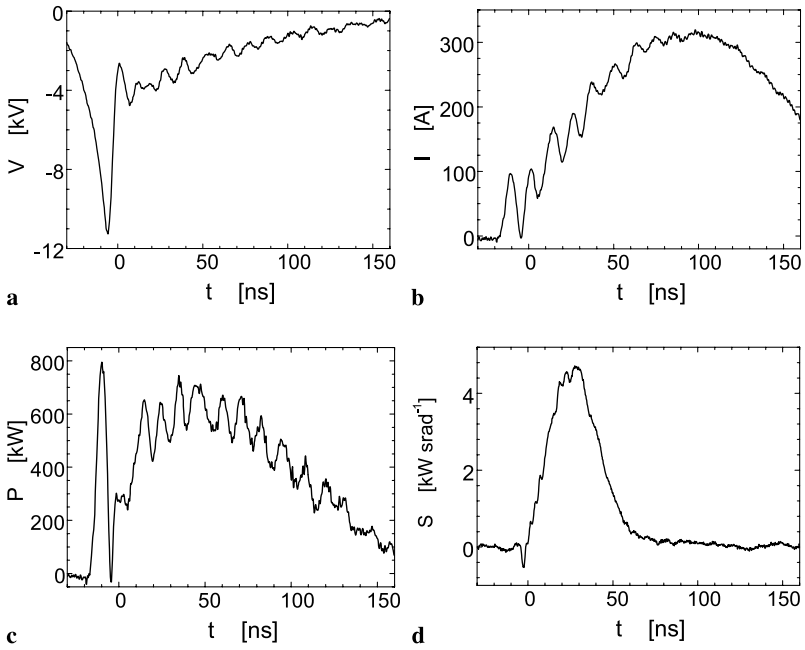

FIGURE 3 Typical measured discharge voltage (**a**) and current (**b**), calculated power deposition (**c**) and measured spontaneous emission (**d**) waveforms. Discharge in a $F_2 : Ar : He$ (0.1% : 5% : 94.9%) mixture at a total pressure of 2 bar and charging voltage 14 kV

higher than 600 kW it stays constant at about 100 ns. The FWHM of the spontaneous emission is almost constant at any pumping power and is about 60 ns with a 10 ns accuracy.

In Fig. 4 the temporal evolution of the net gain $(g-\alpha)L$ is shown in comparison to the spontaneous emission waveform obtained under the same conditions. The delay between the discharge ignition and the probe laser pulse was changed in ~ 10 ns steps, however due to the jitter in the laser pulse the appearance of the actual points are spread around the chosen offset. The open circles (curve 1) represent the real net gain data measured, showing a large shot-to-shot fluctuation. The black dots (curve 2) represent the average values of the net gain and the error bars show the standard deviation of the experimental points. The large shot-to-shot fluctuation of the net gain is due to a number of reasons. The fluctuation of the spontaneous emission signal amplitude is in the order of $\sim 10\%$–15%, as is shown below. This is caused by fluctuations of the discharge volume and the energy deposited into the discharge because the jitter between the X-ray pulse and the discharge ignition results in slightly different starting conditions of the discharge. The fluctuation of the spontaneous emission can also be attributed to the development of small local discharge instabilities not resulting in arcing. In addition, the position of the discharge center may shift from shot to shot with the consequence that the probe beam effectively passes through different parts of the discharge volume. As a result the amplification of the probe laser pulse ($A = (S_c^*/S_r^*)/\langle S_c/S_r\rangle$) shows a 10%–15% shot-to-shot fluctuation. The net gain is determined from (2), where S_c, S_s, S_c^* and S_s^* are measured in the experiments as described above. The logarithm in (2) increases the relative deviation even further. For example, let the pulse amplification $A = A_0 \pm \delta A$, where the average value A_0 is ~ 1.2 and the deviation $\delta A \sim 0.15$. Then $\ln(A) = \ln(A_0 \pm \delta A) \approx \ln(A_0) \pm \delta A/A_0 \approx 0.18 \pm 0.13$. This explains the large spread of the experimental points and vertical error bars, which represent the standard deviation of the averaged values. The horizontal error bars show the standard

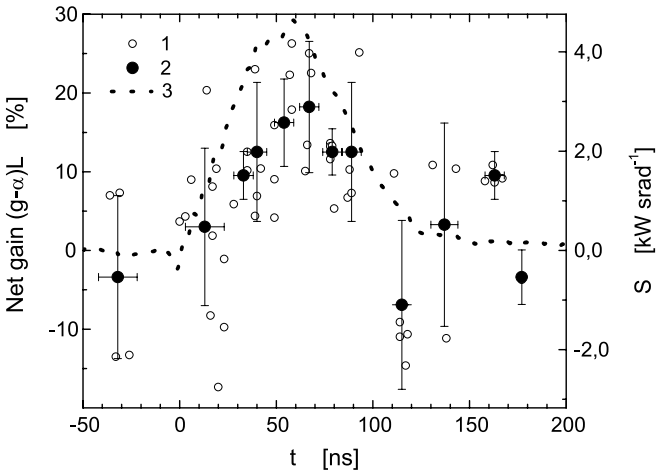

FIGURE 4 Typical measured net gain (1) and averaged net gain temporal profile (2) in comparison with the measured spontaneous emission waveform (3). Discharge in a $F_2 : Ar : He$ (0.1% : 5% : 94.9%) mixture at a total pressure of 2 bar and charging voltage 14 kV

deviation of the points in time due to jitter of the laser pulse. Curve 3 is the spontaneous emission waveform. The discharge is excited in a $F_2 : Ar : He$ (0.1% : 5% : 94.9%) gas mixture at 2 bar total pressure and at a charging voltage of 14 kV. The FWHM of the gain profile is approximately 60 ns, the same as the FWHM of the spontaneous emission waveform. The peak net gain is approximately $16 \pm 8\%$.

The dependencies of the peak net gain $(g-\alpha)L$ and peak spontaneous emission signal on the peak power deposition are shown in Fig. 5 for discharges in $F_2 : Ar : He$ (0.1% : 5% : 94.9%) (1) and $F_2 : He : Ar : Ne$ (0.1% : 1.9% : 5% : 93%) (2) gas mixtures at a total gas pressure of 2 bar. The net gain and the spontaneous emission intensities grow with the increase of the pumping power in both cases. When Ne is used as a buffer gas, the net gain and the spontaneous emission are higher than in gas mixtures with He as a buffer gas at the same power

deposition. In the case of Ne the net gain and the emission intensity reach saturation at a pumping power of approximately 650 kW. In the case of He no saturation was observed. The maximum obtained peak gain is about $20 \pm 8\%$ in both gas mixtures with Ne or He as a buffer gas. The origin of the vertical error bars in the upper part of the figure is the same as in Fig. 4. The vertical error bars in the lower part of the figure show the standard deviation of the measured amplitude of the spontaneous emission. The horizontal error bars are due primarily to the shot-to-shot fluctuation of the power deposition and partially to the electro-magnetic noise, causing the oscillations on the calculated power deposition waveform (see Fig. 3c).

The data shown in Fig. 5 have been normalized to the gas discharge volume and discharge width yielding specific values for the peak net gain and the peak spontaneous emission signals. These dependencies of the specific peak net gain $(g-\alpha)$ and specific peak spontaneous emission signal on the peak power deposition density are shown in Fig. 6. Compared to Fig. 5 a considerable increase of the vertical and horizontal error bars can be seen. This is due to the fluctuation of the discharge width and the uncertainty of its determination. The average discharge width L is measured from discharge photos and the discharge volume scales as L^2. From this figure it can be concluded that the input power density is almost constant for the total range of investigated power inputs for both the He- and Ne-based gas mixtures. The input power density is $\sim 0.9\,\mathrm{MW\,cm^{-3}}$ for Ne-based gas mixtures and $\sim 1.9\,\mathrm{MW\,cm^{-3}}$ for He-based gas mixtures. It can be seen from Fig. 6 that the discharge emits approximately $10\,\mathrm{kW\,srad^{-1}\,cm^{-3}}$ of UV radiation at a wavelength of 193 nm independently of the total power deposition. Therefore, it can be concluded that these discharges appear to behave in the same way as a so-called "normal glow discharge" known from dc gas discharges. With an increase of the charging voltage the total current increases while the discharge expands, however the steady-state voltage and the current density stay constant. The current density is that in the positive column of the discharge, not the cathode sheath current density. Almost the entire volume of the gas discharge in our experiments is occupied by the positive column. Thus the constant voltage drop across the discharge gap and the constant current density indicate that the specific electric field strength E/p is constant. Therefore the specific net gain $(g-\alpha)$ is also expected to be constant for both mixtures and this is confirmed by the experiments shown in Fig. 6. However this is the case only for a high total peak power deposition: > 650 kW in Ne-based and > 800 kW in He-based gas mixtures and when the discharge is broad with a width of about 1 cm.

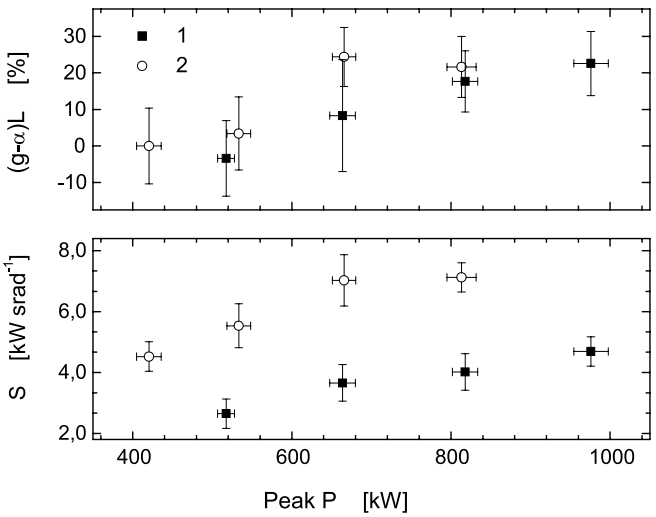

FIGURE 5 Dependencies of the peak net gain $(g-\alpha)L$ and peak spontaneous emission signal on the peak pumping power. Discharges in $F_2 : Ar : He$ (0.1% : 5% : 94.9%) (1) and $F_2 : He : Ar : Ne$ (0.1% : 1.9% : 5% : 93%) (2) gas mixtures at a total gas pressure of 2 bar

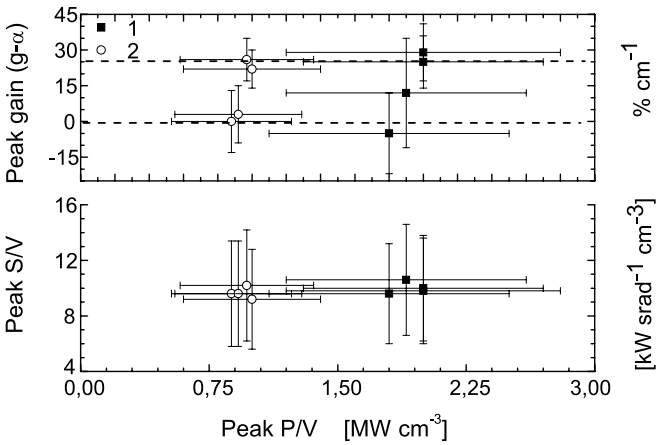

FIGURE 6 Typical dependencies of the specific peak net gain $(g-\alpha)$ and specific peak spontaneous emission signal on the peak pumping power deposition density. Normalized data from Fig. 5. Discharges in $F_2 : Ar : He$ (0.1% : 5% : 94.9%) (1) and $F_2 : He : Ar : Ne$ (0.1% : 1.9% : 5% : 93%) (2) gas mixtures at a total gas pressure of 2 bar

At lower power deposition the discharge is narrower and its width is comparable to the width of the probe beam (3 mm). In this region the specific net gain is much lower, and even close to zero. These results can be explained taking into account the axial symmetry of the discharge and finite widths of the discharge and the probe beam. For a homogeneous gain distribution throughout the discharge, the net amplification of the probe beam exponentially increases with the increase of the beam path through the active medium. The probe beam is sent through the centre of the discharge. For a broad discharge with a width that is significantly wider than the probe beam width, all parts of the probe beam travel almost the same distance through the active medium. In the case of a narrow discharge, the outer parts of the probe beam pass a shorter distance through the discharge than the central part of the beam and consequently the total gain length is lower in this case. If the gain is not distributed homogeneously, for example when it is higher in the centre of the discharge compared to the discharge edges, this effect is more prominent, as a numerical simulation shows. From Fig. 6 it can be seen that the effective specific net peak gain, corresponding to a homogeneous gain distribution, is as high as $\sim 30 \pm 20\%\,\mathrm{cm^{-1}}$.

The spatial gain profile was measured in order to see if the gain distribution was homogeneously distributed. A typical spatial gain distribution profile, measured in a discharge in a $F_2 : Ar : He$ (0.1% : 5% : 94.9%) gas mixture at a total pressure of 2 bar and a charging voltage of 14 kV corresponding to a power deposition of ~ 800 kW, is shown in Fig. 7.

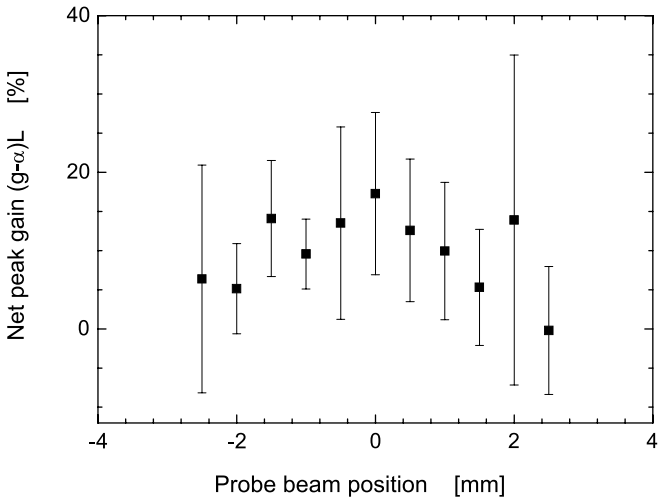

FIGURE 7 Typical averaged peak gain distribution profile measured in discharge in a F_2 : Ar : He (0.1% : 5% : 94.9%) gas mixture at a total pressure of 2 bar and a charging voltage of 14 kV

The probe laser pulse with a diameter of 0.8 mm is applied at the time of the peak of the spontaneous emission signal. Each point presented in Fig. 7 is an average of 10 measurements. The width of the active medium as determined from the gain spatial profile is ∼ 5–6 mm, while the width of the visible discharge glow is ∼ 7–8 mm. The origin of the error bars shown in this figure is the same as in Fig. 4.

4 Conclusion

With a very simple single pulse charge transfer excitation scheme, we obtained a stable discharge in different Ar and F_2 containing excimer laser gas mixtures across a 1 cm gap in a plane-to-plane electrode configuration in a 1 cm diameter X-ray preionized volume. The discharge current and pumping power deposition, the spontaneous emission intensity and the net gain increased with the charging voltage. As the charging voltage increases (from ∼ 8 kV), the discharge cross-section grows with increasing charging voltage until the discharge occupies the entire preionized volume. After the discharge cross-section has become constant, the spontaneous emission and gain saturates but the current and power deposition keeps growing with the increase of the charging voltage.

The observed spontaneous emission intensity and gain depend on the gas mixture composition and total gas pressure. For example, in a discharge in F_2 : Ar : He (0.1% : 5% : 94.9%) at 2 bar and 16 kV charging voltage, a pumping pulse with a peak power deposition of ∼ 1 MW (a specific peak power deposition of ∼ 1 MW cm^{-3} bar^{-1}) and a FWHM of ∼ 100 ns is obtained. This pumping pulse leads to an observed spontaneous emission pulse at a wavelength of 193 nm with a peak intensity of ∼ 4.5 kW srad^{-1} (a specific value of ∼ 10 kW srad^{-1} cm^{-3}) and a FWHM of ∼ 60 ns. The instant conversion efficiency (peak input power to peak emission power) of the deposited electrical energy to UV radiation at this wavelength is ∼ 5.6%, while the total energy efficiency is ∼ 3.4%. This high efficiency indicates that discharge conditions achieved in our setup are very favorable for excimer formation. Such discharges can be used as efficient sources of excimer flash lamps or excimer lasers.

We measured a specific peak net gain value from ∼ 20 ± 10% cm^{-1} (calculated from the measured visible width of the discharge glow) to ∼ 30 ± 20% cm^{-1} (based on the measured width of the spatial gain profile). This specific net gain coefficient is considerably higher than previously reported values [3–5], even taking into account the large experimental errors. The FHWM of the gain waveform is ∼ 60 ns. Therefore, the discharge system presented in this paper is a very promising design for fluorine-based excimer laser applications.

ACKNOWLEDGEMENTS This research was supported by the Technology Foundation STW, the applied science division of NWO and the technology program of the Ministry of Economic Affairs of the Netherlands.

REFERENCES

1 B.W. Smith, Y. Fan, M. Slocum, L. Zavyalova, Proc. SPIE **5754** (2005)
2 M. Ohwa, M. Obara, J. Appl. Phys. **63**, 1306 (1988)
3 S. Watanabe, A. Obara, T. Sato, H. Kashiwagi, Appl. Phys. Lett. **35**, 365 (1979)
4 K. Mossavi, T. Hofmann, G. Szabo, F.K. Tittel, Opt. Lett. **18**, 435 (1993)
5 S.J. Scott, Appl. Phys. B **56**, 201 (1993)
6 F.A. van Goor, J. Phys. D Appl. Phys. **26**, 404 (1993)